Optical Engineering

OpticalEngineering.SPIEDigitalLibrary.org

Effects of temperature inversion in the lower atmosphere on dispersion and angle of arrival of highly directional beams

Mohammad Abdullah-Al-Mamun
David Voelz

SPIE.

Mohammad Abdullah-Al-Mamun, David Voelz, "Effects of temperature inversion in the lower atmosphere on dispersion and angle of arrival of highly directional beams," *Opt. Eng.* **59**(8), 081802 (2020), doi: 10.1117/1.OE.59.8.081802

Effects of temperature inversion in the lower atmosphere on dispersion and angle of arrival of highly directional beams

Mohammad Abdullah-Al-Mamun[a,b,*] **and David Voelz**[a]
[a]New Mexico State University, Klipsch School of Electrical and Computer Engineering, Las Cruces, New Mexico, United States
[b]New Mexico State University, Department of Physics, Las Cruces, New Mexico, United States

Abstract. The performance of free-space optical applications can be improved using beams of different wavelengths for the auxiliary actions of pointing/tracking or turbulence correction. Chromatic dispersion owing to the atmosphere is an issue for multiwavelength systems, and the dispersion of electromagnetic signals is typically predicted based on refractive conditions from standard atmospheric models. However, for long near-horizontal paths near the Earth's surface, substantial refractive index gradients that are associated with features such as inverse temperature layers and ducts can be encountered. These features can significantly alter the ray trajectory, the chromatic divergence, and the angle of arrival of directional beams relative to standard atmosphere predictions. A ray tracing approach was implemented to examine the chromatic divergence and angle of arrival of the rays through various practical and extreme atmospheric conditions involving a temperature inversion layer. Over a distance of 150 km along the ground, a brief encounter with the layer can cause pairs of rays with wavelengths 532 and 1550 nm to diverge up to 4.5 times greater than their standard atmosphere predictions. For a single wavelength, a linear increase of angle of arrival with initial launch angle was found for the standard atmosphere, but this trend was significantly altered in the presence of an inversion layer. Extreme refractive conditions with a large inversion layer were simulated to produce optical ducting over long distances. Chromatic separation of rays as large as 280 m was observed when only one of the two wavelengths remained in the duct. [DOI: 10.1117/1.OE.59.8.081802]

Keywords: anomalous refraction; atmospheric refraction; chromatic dispersion; free-space optics; laser propagation; terrestrial refraction.

Paper 191663SS received Nov. 30, 2019; accepted for publication Feb. 18, 2020; published online Mar. 10, 2020.

1 Introduction

The propagation of an optical signal through the clear atmosphere is affected mainly by atmospheric refraction and turbulence. As light propagates through the Earth's lower atmosphere in a horizontal or near-horizontal direction, refraction is responsible for some of the most interesting atmospheric optical phenomena such as mirages—the Fata Morgana and Novaya Zemlya effects—the green flash, and ducting. These phenomena are usually associated with the formation of significant refractive index gradients close to the ground.

The value of the atmospheric refractive index is close to unity and it varies with temperature, pressure, humidity, altitude, and wavelength of the signal. For the standard atmosphere, the vertical refractive index gradient is $\sim -3.9 \times 10^{-5}$ km^{-1} near the ground at optical frequencies and its magnitude decreases with increasing altitude ($\sim -3.3 \times 10^{-5}$ km^{-1} at 1-km altitude). Overall, this gradient tends to bend the optical path of the light toward the surface of the Earth. Due to the wavelength dependency of the refractive index and its gradient, the amount of bending of the propagating signal is also wavelength dependent. This leads to chromatic dispersion where the ray paths for different wavelengths separate as they propagate. Dispersion in

*Address all correspondence to Mohammad Abdullah-Al-Mamun, E-mail: mamun@nmsu.edu

the atmosphere can generally be ignored for short propagation paths, but it becomes significant for applications such as laser communication or astronomical observation near the horizon, where long propagation paths (tens to hundreds of km) may be involved. Chromatic corrections for these applications are commonly predicted based on the standard atmospheric models. However, the real atmospheric condition may be quite different from the standard models, and unusual features, such as temperature inversion and atmospheric ducts, could significantly affect the chromatic divergence and propagation direction for highly directional beams. Understanding the range of behavior for beams under various dispersion conditions is important when considering correction approaches for applications such as laser communication, LIDAR, target designation, and astronomical observation, where accurate estimation of the propagation path is required for optimum performance.

In this study, we apply a ray tracing algorithm to atmospheric and duct profile models available in the literature that are modified to include a temperature inversion layer. Refractivity of the air as a function of wavelength is modeled with a reduced refractivity coefficient, and a temperature inversion layer is simulated based on a duct profile found in the literature. The chromatic divergence between rays of wavelength 532 nm (green) and 1550 nm (IR) is examined as a function of source height and initial ray trajectory angle relative to the layer position. In certain cases, the encounter with the temperature inversion layer can create significant separation between the rays of different color. The effect of the temperature inversion layer on the angle of arrival (AOA) of the rays at the target location was also studied. Deviation from a linear relationship between the AOA and launch angle was observed as the rays encountered the inversion layer.

2 Theory and Background

2.1 *Chromatic Dispersion in the Atmosphere*

The trajectory of an optical beam propagating through the atmosphere is fundamentally dependent on the dispersion relationship (wavelength dependency of the refractive index) of the air. If the refractive index field for a particular volume of air is known, then the propagation path of an optical beam through the volume can be traced by applying Snell's law of refraction. The atmospheric refractive index profile for dry air can be expressed as[1]

$$n = 1 + A_D(\lambda)\frac{P(h)}{T(h)}, \tag{1}$$

where $P(h)$ and $T(h)$ are the pressure and temperature profiles as a function of altitude (h) and have units of hPa and K, respectively. $A_D(\lambda)$ is the reduced refractivity coefficient for dry air, which is a function of wavelength and is measured in K/hPa units. Several models for the reduced refractivity coefficient have been developed over the years and are available in the literature. For our study, we used Edlén's expression in Sellmeier's form[1,2]

$$A_D(\lambda) = 10^{-8}\left[8342.13 + \frac{2406030}{130 - \frac{1}{\lambda^2}} + \frac{15997}{38.9 - \frac{1}{\lambda^2}}\right]\frac{288.2}{1013.25}, \tag{2}$$

where λ is the wavelength of the propagating signal in μm. The choice of this expression is based on its high accuracy over a relatively large electromagnetic spectral range, from ultraviolet to the IR region.

2.2 *Standard Atmospheric Models*

For numeric simulation of optical ray trajectory through the inhomogeneous atmosphere for a specific wavelength, the altitude-dependent (vertical) refractive index profile is required. From Eq. (1), the vertical refractive index can be obtained from altitude-dependent pressure and temperature profiles. We note that at optical frequencies, the humidity-dependent contribution to the refractive index is very small and can be ignored.[3] The temperature and pressure profiles of the atmosphere are commonly modeled based on geographic reference atmospheric models.

These models are described by a sequence of spherical layers in the lower troposphere with each layer having a constant vertical temperature gradient.

The altitude-dependent atmospheric properties of six commonly cited reference atmospheric models are listed in a tabular form in an Air Force Geophysics Laboratory technical report by Anderson et al.,[4] which is publicly available. These layered atmospheric models assume constant temperature gradients for the vertical temperature profile for each layer. In our simulations, we applied the 1976 U.S. Standard Atmosphere and Subarctic Winter Atmosphere reference models. The Subarctic Winter Atmosphere has the largest temperature gradient among the six reference atmospheric models and hence tends to cause the largest bending of the propagating optical signals. For these atmospheric models, the temperature profile in a given layer in the lower troposphere is modeled as

$$T = T_0 - \alpha h, \tag{3}$$

where T_0 is the mean sea-level temperature, α is the temperature gradient, and h is the altitude in km. For the U.S. Standard Atmosphere, $T_0 = 288.2$ K and $\alpha = 6.5$ K/km. For the Subarctic Winter Atmosphere, $T_0 = 257.2$ K and $\alpha = 18.1$ K/km (for the first km from sea level). These models of the atmosphere are strictly a function of altitude, and hence the temperature and refractive index profiles vary only in the vertical direction. Applying this temperature profile, the pressure profile with altitude is then obtained as follows:[5]

$$P(h) = P_0\left(\frac{T_0 - \alpha h}{T_0}\right)^{\frac{M_a g}{R\alpha}}, \tag{4}$$

where P_0 is the sea-level atmospheric pressure in hPa units (1013.25 hPa), M_a is the mean molar mass of air molecules in gm/mol, $g = 9.81$ ms^{-2} is the gravitational acceleration, and $R = 8.3144$ JK^{-1} mol^{-1} is the ideal gas constant.

Inserting Eqs. (3) and (4) into Eq. (1), we get the following expression for the atmospheric refractive index profile:

$$n(\lambda, h) = 1 + A_D(\lambda)\frac{P_0}{T_0}\left(\frac{T_0 - \alpha h}{T_0}\right)^{\frac{M_a g}{R\alpha}-1}. \tag{5}$$

Considering the reduced refractivity $A_D(\lambda)$ to be independent of the altitude, an expression for the refractive index gradient can be obtained analytically, and it is given as

$$\frac{dn}{dh}(\lambda, h) = -A_D(\lambda)P_0 T_0^{-\frac{M_a g}{R\alpha}}\left(\frac{M_a g}{R} - \alpha\right)(T_0 - \alpha h)^{\left(\frac{M_a g}{R\alpha}-2\right)}. \tag{6}$$

2.3 *Refractivity, Effect of Earth Curvature, Modified Refractivity, and Refractive Conditions*

The value of the refractive index of the atmosphere is close to unity, and its value varies slowly in the vertical direction for the reference atmospheric models. Therefore, the refractive index at optical frequencies only changes in the fifth to sixth decimal places over the visible spectra. Hence, it is convenient to use the quantity:

$$N = (n - 1) \times 10^6 \ (N - \text{units}), \tag{7}$$

which is known as the refractivity. The refractive index gradient is related to the gradient of the refractivity by

$$\frac{dn}{dh} = \frac{dN}{dh} \times 10^{-6}. \tag{8}$$

For long horizontal or low-angle optical propagation, the refractivity model should include the curvature of the Earth. Optical signals traveling at low grazing angles tend to move away

from the Earth's surface due to the Earth's curvature. To account for this effect and simplify the analyses, the modified refractivity (M) is used, where it is given as

$$M = N + \left(\frac{h}{R_E}\right) \times 10^6 = N + 157 \times h \ (M - \text{units}), \tag{9}$$

where h is the altitude in km from the Earth's surface and R_E is the Earth's radius in km. The mean radius of the Earth is calculated to be ~6371 km by International Union of Geodesy and Geophysics, and this value was used in Eq. (9).[6] As we are primarily concerned with horizontal or nearly horizontal propagation of optical beams, we used the modified refractivity and its gradient in our numeric simulation model.

In numerical modeling, the gradient of the modified refractivity is used to simulate actual ray trajectory for horizontal and low-angle optical signal propagation. Based on the modified refractivity gradient values, the refractive conditions can be divided into four categories (Fig. 1).[7,8] For radar or optical ray tracing, when $\partial M/\partial h > 157$ M-units/km, rays will propagate away from the Earth's surface, and this is referred to as the subrefraction condition. When 157 M-units/km $\geq \partial M/\partial h > 118$ M-units/km, standard wave propagation occurs, and this is known as the standard condition. With 118 M-units/km $\geq \partial M/\partial h > 0$ M-units/km, rays bend downward, and this condition is termed as super-refraction. In ducting/trapping condition where $\partial M/\partial h \leq 0$, the rays (particularly for radar) can become trapped between the ground and the ducting layer. As a point of comparison, for the standard condition, the radio refractivity gradient dN/dh is ~ -40 N-units/km near the Earth's surface whereas for the visible spectra the value is ~ -39 N-units/km.

For our study, we are particularly interested in the super-refraction and ducting region as the temperature inversion layer creates strong negative refractivity gradients for optical frequencies. The gradients in the ducting layer or temperature inversion layers can give rise to chromatic dispersion and significantly impact the propagation path of optical signals. The inversion layer parameters for this study were chosen based on experimental results from time-lapse camera measurements that were carried out in Las Cruces, New Mexico.[9] Generally, the U.S. Standard Atmosphere with the modeled temperature inversion layer produces the super-refraction condition for our simulations. To study extreme atmospheric refractive conditions, we also slightly modified and applied the aforementioned temperature inversion profile to the Subarctic Winter Atmosphere. Under certain conditions, ducting of optical signals in the vicinity of the inversion layer was observed in our subarctic winter results.

2.4 *Temperature Inversion, Atmospheric Ducts and Webster Duct Model*

In layered tropospheric models, such as 1976 U.S. Standard or Subarctic Winter models, the temperature is usually highest near the ground and generally decreases with altitude. Tempera-

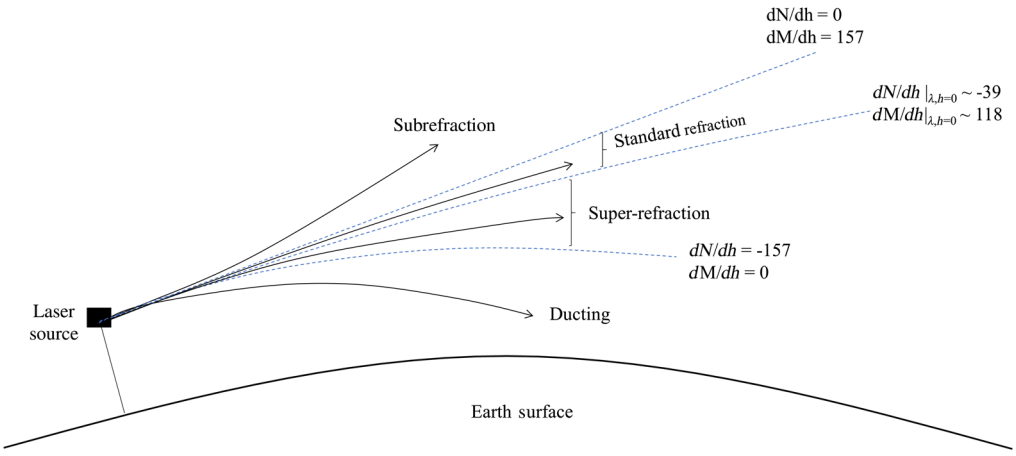

Fig. 1 Illustration of common atmospheric refractive conditions (after Zeng et al.[7]).

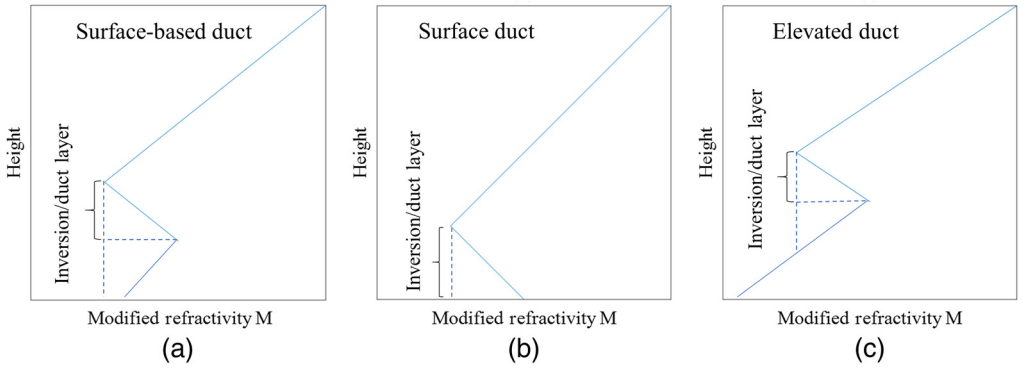

Fig. 2 Modified refractivity profiles for (a) surface-based duct, (b) surface duct, and (c) elevated duct for a simplified atmospheric model with linear vertical refractive index gradient (after Dinc and Akan[8]).

ture inversion occurs when this trend is broken and the temperature increases with altitude. A hot layer of air can become trapped between two relatively cold layers to form a temperature inversion layer, and such a structure can extend over hundreds of kilometers along the ground. Conditions such as rapid cooling of the Earth's surface and the adjacent air early in the night or adiabatic compression of sinking air over the land due to certain regional geographic features can create these sandwiched temperature layers. The denser (cool) air usually has a higher refractive index than the rarer (hot) layer of air in the troposphere. A sufficiently high gradient can trap optical/electromagnetic signals by creating a propagation channel where the rays swing up and down within the atmosphere between the ducting layer and Earth's surface. This phenomenon is known as ducting or trapping. The presence of temperature inversion layers over long distances can lead to propagation channels or ducts for optical/electromagnetic signals and could increase the range of radio signals to over thousand miles with very low path loss.

Based on their formation process and modified refractivity profiles, the atmospheric ducts are commonly classified into four types: evaporation ducts, surface-based ducts, elevated ducts, and surface ducts.[8] Generally, the modified refractivity for evaporation ducts is modeled with log-linear function whereas surface-based and elevated ducts are modeled as a trilinear curve and the surface ducts are modeled with a bilinear curve. Evaporation ducts are particularly important in radio refractivity as radio signals interact with the polarity of water vapor molecules. Thus, radio refractivity is a strong function of relative humidity.[3,10] For optical signals, humidity has a negligible effect, so evaporation ducts are ignored for our study.[3] Figure 2 shows representative refractivity profiles of three duct types, excluding the evaporation duct.

There are several detailed analytical models available in the literature describing the form of the inversion profile for the duct types mentioned above. For our study, we chose the Webster duct profile[11] and applied this profile in the surface-based, elevated, and surface duct types to examine their effect on chromatic dispersion. The Webster duct model, introduced by Webster,[11] was later modified by Grabner and Kvicera,[12] where the refractivity profile is defined by the following equation:

$$N(h) = N_0 + G_N h + \frac{\Delta N}{2} \tanh\left[\frac{2.96(h - h_0)}{\Delta h}\right], \tag{10}$$

where N_0 is the refractivity at sea level and G_N is a wavelength-independent linear vertical gradient approximation for the overall refractive index profile. The third term on the right side of the expression represents the duct profile, where ΔN is the duct depth, h_0 is the duct height, and Δh is the duct width. As our purpose is to study the chromatic dispersion, we used the wavelength-dependent refractivity profile obtained from Eq. (5) along with the duct profile described in Eq. (10). With this modification, the refractivity profile was obtained to be

$$N(\lambda,h)=\left[A_D(\lambda)\frac{P_0}{T_0}\left(\frac{T_0-\alpha h}{T_0}\right)^{\frac{Mg}{R\alpha}-1}\right]\times 10^6+\frac{\Delta N}{2}\tanh\left[\frac{2.96(h-h_0)}{\Delta h}\right]. \quad (11)$$

Taking the Earth's curvature into consideration, the wavelength- and altitude-dependent modified refractivity then becomes

$$M(\lambda,h)=\left[A_D(\lambda)\frac{P_0}{T_0}\left(\frac{T_0-\alpha h}{T_0}\right)^{\frac{Mg}{R\alpha}-1}\right]\times 10^6+\frac{\Delta N}{2}\tanh\left[\frac{2.96(h-h_0)}{\Delta h}\right]+157\times h. \quad (12)$$

For the simulations results presented here, we used a parameterization of the Webster duct model published by Wijerathna et al.[9] These authors analyzed time-lapse imagery, and the results suggested that a temperature inversion-type of layer was present in the early morning at their location in New Mexico. Parameters for the Webster duct model were obtained by a fitting approach associated with the image shift results. For five consecutive mornings in late November, 2014, these authors found the mean of the calculated duct width to be $\Delta h = 48.5$ m and the duct height was found to be $h_0 = 10.8$ m. The parameters were calculated for the time of the day where the maximum image stretching (distortion) was observed and the authors assumed ΔN to be -2 N-units. This profile represents a surface-based temperature inversion profile. The three temperature inversion profiles (surface, surface-based, and elevated) were modeled in our simulations by changing the position of the duct height h_0.

3 Simulation and Results

3.1 *Ray Tracing Method and Algorithm*

When refraction effects are much larger than diffractive effects, light propagation through an inhomogeneous media can be simulated using ray tracing methods. This condition generally holds for the propagation path and refractive features that we are studying. The ray trajectory is usually described by the solution of the eikonal equation.[13–17] A commonly used solution involves the application of a linear transfer equation coupled with a bending equation. The bending equation determines the change in ray trajectory and is a function of change in refractive index between two layers. Starting with Snell's law of refraction,

$$n_1 \sin\theta_1 = n_2 \sin\theta_2 \quad (13)$$

and applying the small-angle approximation, $\sin\theta \approx \theta$, leads to

$$n_1\theta_1 = n_2\theta_2 \quad (14)$$

The small-angle approximation holds for our numeric simulations as the rays travel in a horizontal/near-horizontal path, with a total angular change of ~20 mrad over a 150-km path along the ground. The bending equation between layers is obtained from Eq. (14) as

$$\theta_2 = \frac{n_1}{n_2}\theta_1. \quad (15)$$

With index j for discrete layers, the bending equation for the numeric simulation is

$$\theta_j = \frac{n_{j-1}}{n_j}\theta_{j-1}. \quad (16)$$

The rays are assumed to follow a linear path between planes with the linear transfer equation given as

$$h_j = h_{j-1} + \theta_{j-1}\Delta x_{j-1}, \quad (17)$$

where two-dimensional (2-D) ray propagation is considered and Δx_{j-1} is the horizontal step size for the numeric simulation. To obtain accurate ray trajectories with this approach in a medium

with significant index gradients, relatively small step sizes are required in both vertical and horizontal planes. Ray height h is considered in the vertical direction. Hence, although simple, this numerical model for ray tracing is not time efficient when long paths (tens to hundreds of kilometers) are considered.

Our problem of interest involves refractive index gradients defined in the vertical direction and ray trajectories at low angles relative to the horizontal. For this situation, a second-order ray tracing algorithm[18] was developed that relaxes the step size constraint and allows for faster but accurate ray trajectory calculation. We implemented this second-order ray tracing method in our simulation, where a quadratic correction term is introduced to the transfer equation. This term comes from the solution of a 2-D form of the eikonal equation describing the ray trajectory in an inhomogeneous media. The eikonal equation is given as

$$\frac{d^2h}{dx^2} = \frac{1}{n(h)}\frac{dn}{dh}. \tag{18}$$

For a sufficiently small step size, we can consider the gradient $dn/dh = \kappa$ to be a constant. If we assume $n(h) \approx 1$, the solution of Eq. (18) becomes

$$h(x) = \frac{x^2\kappa}{2} + \theta_0 x + h_0, \tag{19}$$

where h_0 is the initial ray height and θ_0 is the initial angle. Note that h_0 is used here by convention and is not the same variable defined for the layer in Eq. (10). Using Eq. (19) as the transfer equation between the layers, the bending equation can be obtained by taking its derivative, given as

$$\frac{dh}{dx} = \theta(x) = x\kappa + \theta_0. \tag{20}$$

For numeric simulations, the transfer equation [Eq. (19)] and bending equation [Eq. (20)] can be rewritten as follows:

$$h_j = \frac{\Delta x^2 \kappa_{j-1}(h)}{2} + \theta_{j-1}\Delta x + h_{j-1} \tag{21}$$

and

$$\theta_j = \Delta x \kappa_{j-1}(h) + \theta_{j-1}, \tag{22}$$

respectively. The additional term in the transfer equation models a curved ray trajectory between the steps that gives an accurate ray height approximation with fewer iterations, thus reducing the computational time. This is particularly important in our study as the rays propagate through the inhomogeneous atmosphere over a very large distance along the ground.

3.2 *Chromatic Dispersion Simulation Results*

The chromatic dispersion between rays with wavelength 532 and 1550 nm was simulated using the second-order ray tracing algorithm for several practical atmospheric conditions for a distance of 150 km along the ground. Figure 3 provides an example of how the presence of an elevated inversion layer, described by the Webster duct model, impacts the ray trajectory and chromatic divergence.

Figure 3(a) shows ray trajectories through the U.S. Standard Atmosphere gradient profile. Three pairs of 532- and 1550-nm rays are traced from left to right, and the apparent upward trajectory of the rays beyond the 100-km distance is an effect related to the curvature of the Earth's surface. Each pair is launched at a slightly different downward initial angle and as the rays traverse the atmosphere, the 532-nm wavelength rays bend more toward the ground than the 1550-nm rays. Because the refractivity gradient is altitude dependent (indicated by the color bar), the overall amount of ray bending is primarily dependent on the source altitude. Figure 3(b)

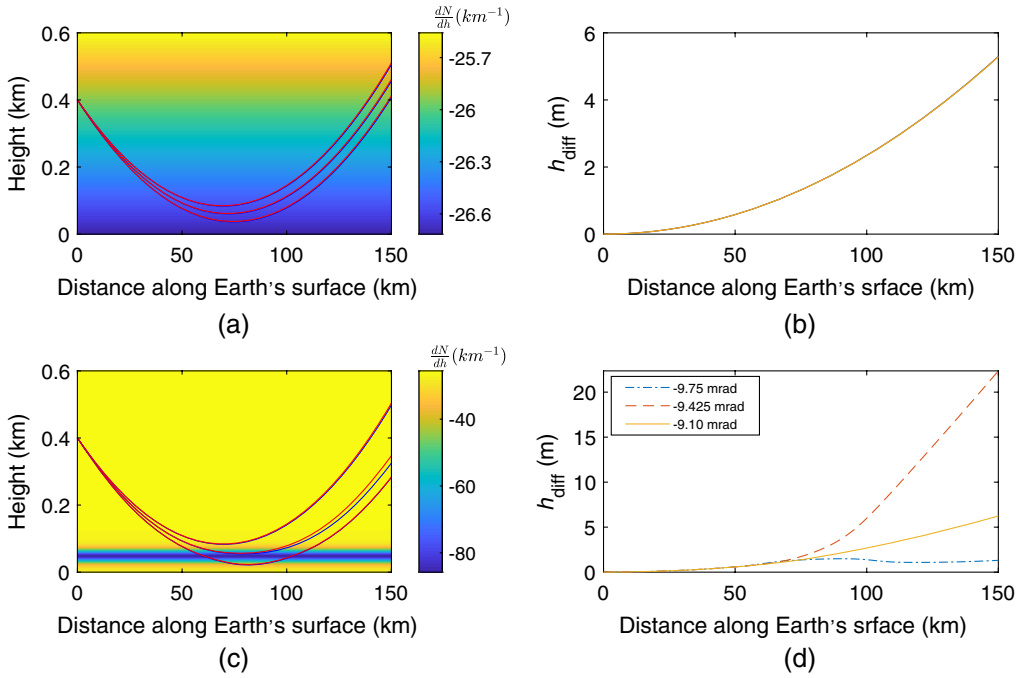

Fig. 3 Ray trajectories of three pairs of 532 nm (blue) and 1550 nm (red) rays where the rays within a pair have the same initial launch angle of −9.75, −9.425, or −9.1 mrad: (a) standard atmosphere and (c) with the temperature inversion. Color bars show the refractivity gradient dN/dh in km^{-1} at 532 nm. The separation between ray pairs as a function of the distance along the Earth's surface for (b) standard atmosphere and (d) with the inversion layer.

shows the separation between rays within a pair (h_{diff}) as a function of distance along the Earth's surface. Regardless of the slight launch angle difference, the rays for this case diverge about 5 m within each pair at the 150-km distance along the Earth's surface in the standard atmosphere. In general, we find for the standard atmosphere case that h_{diff} is also primarily a function of source altitude, where the separation becomes smaller as the source is moved higher in altitude.

However, if the source is located above the inversion layer [Fig. 3(c)], then the shorter wavelength ray encounters the layer feature earlier (in terms of distance along the Earth's surface) than the longer wavelength. This can separate the rays with different colors further or even bring them closer to their standard atmospheric prediction, depending on several factors. Figure 3(d) shows chromatic separation between ray pairs launched at the same angles as in Fig. 3(a) but in the presence of the inversion layer. The ray separation depends on the relative source position with respect to the inversion layer, launch angle, and wavelength of the source. For the case shown in Fig. 3, the separation can be as large as 23 m, which is significantly larger than the ∼5-m prediction for the standard atmosphere.

Figure 4 presents ray separation results for packets of 101 pairs of rays, where each pair is aimed at a slightly different angle toward the inversion layer. Results are shown for source locations below, inside, and above the inversion layer. For a specific source height (h_s), ray packets were launched over an angular range of a few milliradians, such that the rays would encounter the inversion layer. Figure 4 shows ray separation as a function of distance along the Earth's surface for four source altitudes. For the case in Fig. 4(a) with the source below the layer, the result for the ray packet is essentially the same as Fig. 3(b) without the layer. The other cases illustrate that the largest separation effects occur when the source is above the layer and the rays are launched at larger initial angles.

For all of the results in Sec. 3.2, the elevated temperature inversion layer was modeled using the following Webster duct parameter values: $\Delta N = -2$ N units, $\Delta h = 50$ m, $h_0 = 50$ m. The value of the duct width Δh was 50 m (average value is 48.5 m in the work by Wijerathna et al.[9]) and the duct height value $h_0 = 50$ m (average value is 10.8 m in the work by Wijerathna et al.[9]) was used to model an elevated inversion layer to ensure maximum possible interaction of the propagating rays with the inversion layer. This profile coupled with U.S. Standard Atmosphere

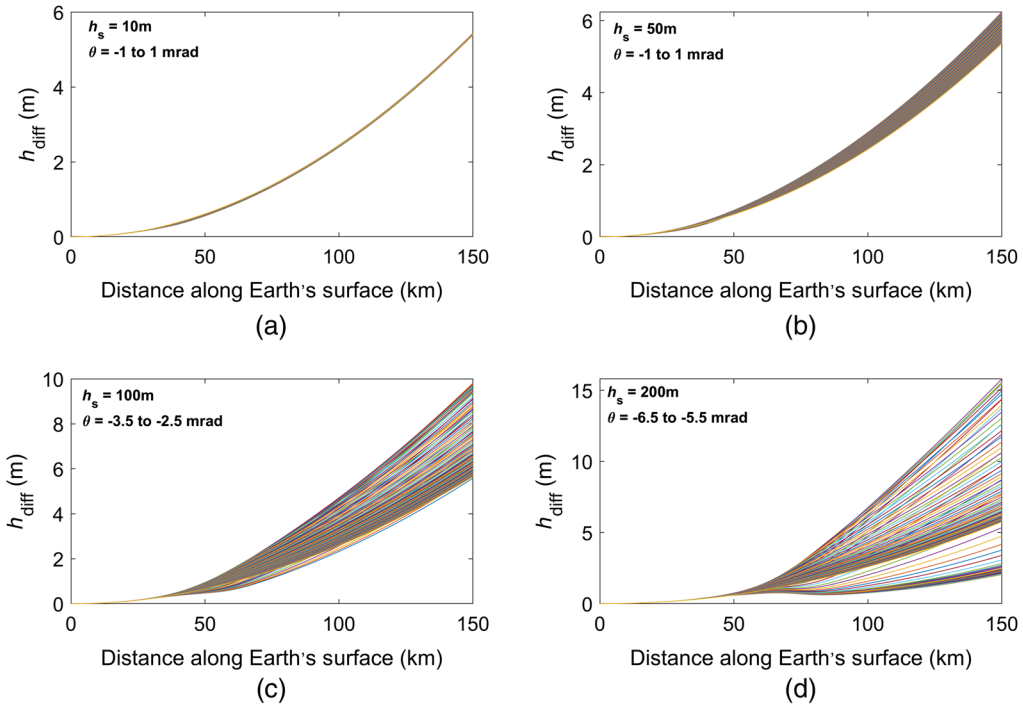

Fig. 4 With the same index gradient profile as Fig. 3(c), the ray separation h_{diff} for 101 pair of rays of 532- and 1550-nm wavelength with four different source locations are shown as a function of distance along the Earth's surface. The rays within each pair have the same launch angle. The source height h_s and launch angle range are (a) 10 m, −1 to 1 mrad; (b) 50 m, −1 to 1 mrad; (c) 100 m, −3.5 to −2.5 mrad; and (d) 200 m, −6.5 to −5.5 mrad.

does not produce a strong enough gradient for ray trapping or ducting but rather corresponds to a super-refraction refractive condition. We ran simulations with different h_0 values to model surface and surface-based duct type inversion layers as well. Our simulations show that the ray separation h_{diff} can be considered independent of the duct type but strongly dependent on the relative distance between the source height (h_s), duct height (h_0), and launch angle.

For the source located above the inversion layer, we ran simulations with the 532-nm wavelength rays to study the ray AOA at the 150-km distance as a function of launch angle. For the standard atmosphere, the AOA increases essentially linearly with increasing launch angle for a particular source height. However, in the presence of an inversion layer, this general trend is broken and the AOA can decrease with increasing launch angle. Figure 5(a) illustrates the dependence of the AOA on launch angle in the standard atmosphere, and Fig. 5(b) shows the effect of the elevated inversion layer (as defined above) on the AOA with the source located at $h_s = 200$ m and rays launched at angles between −6.5 and −5.5 mrad.

3.3 *Ducting and Dispersion Simulation Results Under Extreme Conditions*

Observation of ducting of radio signals goes back as early as World War II, and such anomalous refraction is linked with temperature inversion and the evaporation duct.[19] Hence, it is a curious question to ask whether ducting of optical signals is a possibility. As humidity has a negligible effect on optical signal propagation, we found that a large temperature gradient along with a large temperature inversion is required for optical ducting. The subarctic winter atmospheric profile exhibits a large temperature gradient with height, and literature suggests that large temperature inversion profiles can exist in the subarctic regions.[20,21] Thus, the subarctic region could produce atmospheric conditions that support optical ducting. To examine this possibility, we applied our simulation approach to the Subarctic Winter Atmosphere model with an embedded temperature inversion. Currently, we do not have data for the parametrization of duct profiles for the subarctic atmosphere and we did not find suitable analytic subarctic inversion models for use in our

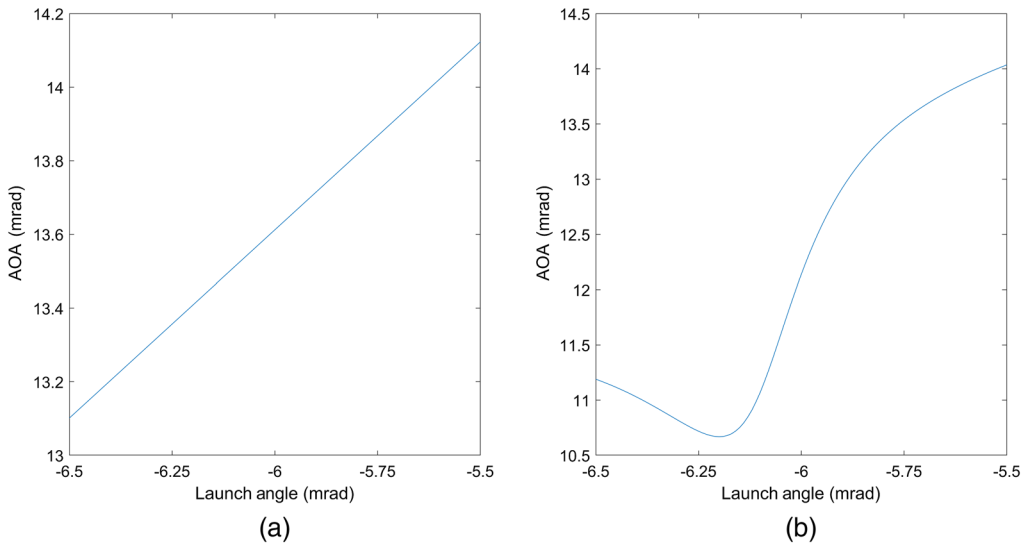

Fig. 5 AOA at the detector location as a function of launch angle for 532-nm source (a) in the U.S. Standard Atmosphere and (b) in the presence of the inversion layer.

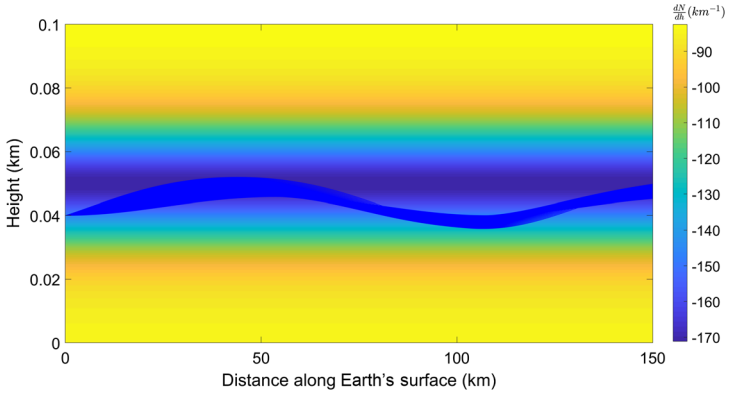

Fig. 6 Ducting of green (532 nm) rays in the subarctic winter atmosphere in the presence of the Webster-type inversion layer (as described in Sec. 3.2 but with $\Delta N = -3$ N units) with the source located at 40 m height and rays launched at 0- to 0.4-mrad angle.

approach. Hence, we applied a temperature inversion layer identical to the one described in Sec. 3.2 to the Subarctic Winter Atmosphere with a change in the parameter $\Delta N = -3$ N units to simulate a stronger inversion. This inversion layer along with the subarctic winter refractive index profile created conditions that cause actual ducting of the optical signal. Figure 6 shows the ducting effect for 101 green (532 nm) rays launched near the center ($h_s = 40$ m) of the ducting layer (duct height = 50 m) with initial launch angles ranging from 0 to 0.4 mrad. The ducting of rays limits the chromatic divergence as long as the rays of different wavelength are all trapped. However, our simulation studies show that for specific source altitudes there can exist an angular launch range over which rays with one color can become trapped by the ducting layer and the rays of the other color may not meet the ducting condition. The chromatic separation between 101 pair of 532- and 1550-nm rays is shown in Fig. 7 for the ducting case described above, with different launch angle ranges and the source located at 40 m above the ground. Chromatic separation is small after the 150-km propagation distance when both colors are ducted [Fig. 7(a)], but for larger launch angles, the 1550-nm rays leave the duct and chromatic separations up to 280 m are demonstrated [Fig. 7(b)]. Although the temperature inversion layer for this example is *ad hoc*, it illustrates the parameters required to produce optical ducting and extreme chromatic separation.

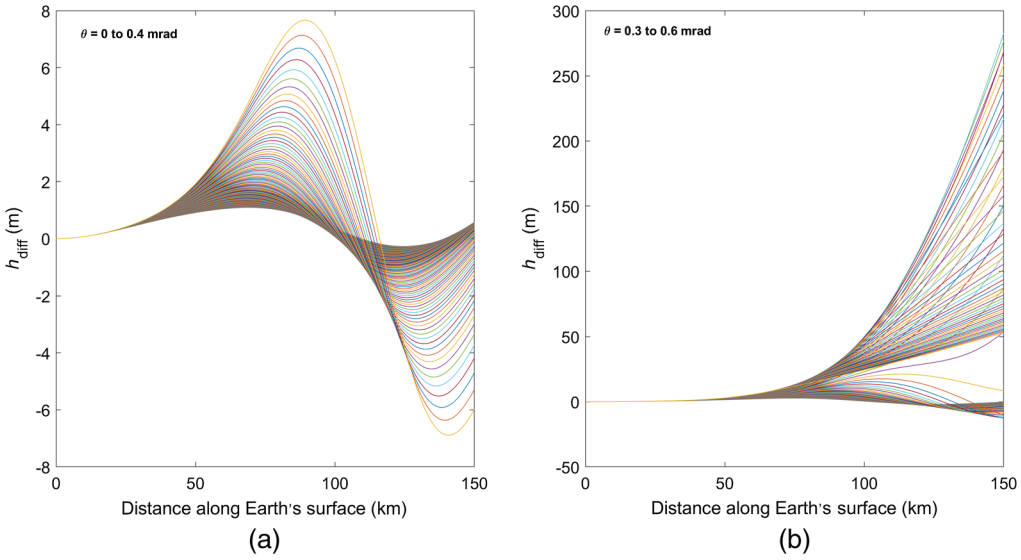

Fig. 7 Chromatic separation between 101 pair of rays of 532- and 1550-nm wavelength as a function of distance along the Earth's surface with the source located at 40-m height in the presence of the inversion layer (as described in Sec. 3.2 but with $\Delta N = -3$ N units) and the subarctic winter atmosphere. Ray launch angles are between (a) 0 to 0.4 mrad, showing ducting of both wavelengths, and (b) 0.3 to 0.6 mrad, where the 1550-nm light leaves the duct for the larger angles.

4 Conclusions

A ray tracing simulation was developed to study the wavelength dependence (dispersion) of optical propagation through atmospheric refractive index features. The dispersion is incorporated through a reduced refractivity coefficient in a modified refractivity expression, and a second-order ray tracing algorithm is applied for improved efficiency and accuracy. Trajectory altitude differences for 532- and 1550-nm wavelength rays were compared using the simulation. We find that for standard atmosphere refraction conditions, the separation between the rays depends largely on the altitude of the source and is nearly independent of the launch angle (for near-horizontal rays with initial angles in milliradians). The chromatic separation becomes smaller as the source is moved higher in altitude.

The presence of a temperature inversion layer introduces significantly higher gradients than the standard atmosphere and can cause much more ray separation (factor of 4.5) than the standard atmosphere depending on the relative source position with respect to the inversion layer, launch angle, and wavelengths of the source. For the inversion layer we studied, we find that the largest ray separation effects occur when the source is above the layer and the rays are launched at relatively larger initial angles. It is important to note that the divergence of chromatic dispersion from the standard atmospheric model in the presence of an inversion layer becomes much more significant when long propagation distances ($\geq$100 km) are involved. The AOA at the detector location increases linearly with increasing launch angle at the source location for the standard atmosphere. However, in the presence of an inversion layer, this trend is broken. It seems possible that this response can be used as an indicator of the presence of such a layer.

We found that the application of the Subarctic Winter Atmosphere model with the addition of a large temperature inversion structure allows for optical ducting and extreme chromatic dispersion. For a source height near the layer height and over a small launch angle window, ducting of the optical signal of one color (532 nm) can occur while the rays of the other color (1550 nm) do not duct. This leads to significant chromatic dispersion, and the simulation produced ray altitude differences as large as 280 m for the 150-km propagation distance.

Acknowledgments

Earlier results of this work appeared in the conference proceedings paper: M. Abdullah-Al-Mamun and D. Voelz, "Chromatic refraction in the lower atmosphere associated with refractive index gradient features," Proc. SPIE 11133, Laser Communication and Propagation through the Atmosphere and Oceans VIII 2019, 11133-12 (13 August 2019). This work was supported by the Directed Energy Joint Transition Office (DE JTO); Award No. N00014-17-1-2535.

References

1. S. Y. van der Werf, "Ray tracing and refraction in the modified US 1976 atmosphere," *Appl. Opt.* **42**(3), 354–366 (2003).
2. B. Edlén, "The refractive index of air," *Metrologia* **2**(2), 71–80 (1966).
3. H. W. Ko, J. W. Sari, and J. P. Skura, "Anomalous microwave propagation through atmospheric ducts," *Johns Hopkins APL Tech. Digest* **4**(1), 12–26 (1983).
4. G. P. Anderson et al., "AFGL atmospheric constituent profiles (0–120 km)," Technical Report AFGL-TR-86-0110, Optical Physics Division, Air Force Geophysics Laboratory (1986).
5. M. N. Berberan-Santos, E. N. Bodunov, and L. Pogliani, "On the barometric formula," *Am. J. Phys.* **65**(5), 404–412 (1997).
6. H. Moritz, "Geodetic reference system 1980," *Bull. Géodésique* **54**(3), 395–405 (1980).
7. Y. Zeng, "Radar beam tracing methods based on atmospheric refractive index," *J. Atmos. Oceanic Technol.* **31**, 2650–2670 (2014).
8. E. Dinc and O. B. Akan, "Channel model for the surface ducts: large-scale path-loss, delay spread, and AOA," *IEEE Trans. Antennas Propag.* **63**(6), 2728–2738 (2015).
9. E. Wijerathna, D. Short, and D. Voelz, "Time lapse image stretch measurements to obtain atmospheric refractivity duct model parameters," in *Proc. OSA Imaging and Appl. Opt.*, Paper PTu2D.2 (2017).
10. E. K. Smith, Jr. and S. Weintraub, "The constants in the equation for atmospheric refractive index at radio frequencies," *J. Res. Nat. Bur. Stand.* **50**(1), 39–41 (1953).
11. A. R. Webster, "Raypath parameters in tropospheric multipath propagation," *IEEE Trans. Antennas Propag.* **30**(4), 796–800 (1982).
12. M. Grabner and V. Kvicera, *Electromagnetic Waves*, pp. 139–156, InTechOpen, United Kingdom (2011).
13. B. E. A. Saleh and M. C. Teich, "Ray optics," Chapter 1 in *Fundamentals of Photonics*, John Wiley & Sons, Inc., Hoboken, New Jersey (2007).
14. B. E. A. Saleh and M. C. Teich, "Wave optics," Chapter 2 in *Fundamentals of Photonics*, John Wiley & Sons, Inc., Hoboken, New Jersey (2007).
15. B. E. A. Saleh and M. C. Teich, "Fiber optics," Chapter 9 in *Fundamentals of Photonics*, John Wiley & Sons, Inc., Hoboken, New Jersey (2007).
16. E. W. Marchand, "Axial gradients," Chapter 4 in *Gradient Index Optics*, Academic Press, New York (1978).
17. E. W. Marchand, "Radial gradients," Chapter 5 in *Gradient Index Optics*, Academic Press, New York (1978).
18. D. J. Short, "Refraction in the lower troposphere: higher order image distortion effects due to refractive profile curvature," PhD Dissertation, New Mexico State University (2016).
19. H. V. Hitney et al., "Tropospheric radio propagation assessment," *Proc. IEEE* **73**(2), 265–283 (1985).
20. H. Ueno and I. Yasuda, "Temperature inversions in the subarctic North Pacific," *J. Phys. Oceanog.* **35**, 2444–2456 (2005).
21. M. A. Bilello, "Survey of Arctic and subarctic temperature inversions," Technical Report, 161, U.S. Army Materiel Cammand, Cold Region Research and Engineering Laboratory, Hanover, New Hampshire (1966).

Mohammad Abdullah-Al-Mamun is a research assistant in the Klipsch School of Electrical and Computer Engineering, New Mexico State University (NMSU). He received his BS and MS

degrees in physics from the University of Dhaka, Bangladesh. He also received an MS degree in physics from NMSU in 2018. His research interests include laser propagation through the atmosphere, atmospheric turbulence, adaptive optics, and optical system design. He is a student member of SPIE.

David Voelz is a professor in the Klipsch School of Electrical and Computer Engineering, NMSU. His research interests include optical propagation through turbulence, spectral and polarization sensing, imaging theory, astronomical instrumentation development, and laser communications. He received his PhD in electrical engineering from the University of Illinois in 1987. He is a fellow of SPIE and OSA.